2018 25th International Lightning Detection Conference &
7th International Lightning Meteorology Conference
March 12 - 15 | Ft. Lauderdale, Florida, USA

Recovery of Valuable Incompletely-Recorded Return-Stroke Current Derivative Signals

Lakmini Perera
Electrical and Computer Engineering Department
Ryerson University
Toronto, Canada
lakmini.perera@ryerson.ca

Ali M. Hussein
Electrical and Computer Engineering Department
Ryerson University
Toronto, Canada
ahussein@ee.ryerson.ca

***Abstract*—Researchers have studied a number of simulating functions for modelling CN Tower lightning return-stroke current. They found out that Heidler and the Pulse functions overcome certain limitations, including time-derivative discontinuities. On the other hand, incompletely-recorded current derivative signals represented another challenge. The paper proposes a double-term Pulse function that is investigated and compared with the double-term Heidler function for modelling the lightning return-stroke current. The double-term simulating function, used to recover a large incompletely-recorded return-stroke current derivative signal measured on June 10, 1996.**

Keywords—Heidler function, Pulse function, lightning return-stoke current, signal recovery

I. INTRODUCTION

Lightning has been one of the most intriguing phenomenon known to man. Benjamin Franklin started investigating electricity in 1746. In 1752, during a thunderstorm, Franklin conducted his famous experiment when he flew a kite with a conducting string and a key tied to the bottom of the kite. During a thunderstorm, he observed sparks flying from the key tied to the conducting kite string and onto his knuckles. This experiment proved that thunderclouds are electrically charged and lightning is electrical [Uman, 1971]. Despite its spectacular nature, lightning has a long record of catastrophic damages, especially for tall objects. Study of lightning has helped in protecting tall structures, forests and powerlines [Hussein et al., 1995; Janischewskyj et al., 1997]. The Canadian National (CN) Tower located in Toronto, 553m in height, has been pivotal to the emergence of lightning studies at the University of Toronto and Ryerson University. It provides a suitable object for recording tall-structure lightning parameters. Although the lightning flash density in Toronto is about 2.5/km^2/year, the CN Tower normally receives dozens of direct strikes yearly [Janischewskyj et al., 1997]. In the past, researchers did investigate a number of simulating functions for modelling CN Tower lightning return-stroke current, including the double-exponential and Jones modified double-exponential functions. However, these functions were found to have problems due to their time-derivative discontinuities [Heidler and Cvetic, 2002; Jones, 1977]. On the other hand, Heidler and the Pulse functions were used to overcome these limitations [Elrodesly and Hussein, 2012; Yazhou et al., 2002]. Other challenges were early noted due to reflections from CN Tower's structural discontinuities [Hussein, 2009; Hussein et al., 2014; Rahimian and Hussein, 2015] and the interfering Loran-C Signal [Liatos and Hussein, 2005; Nedjah, et al., 2010]. Furthermore, the incompletely recorded current derivative signals, which exceeded the maximum signal set level, represented another challenge [Rahimian and Hussein, 2015]. In fact these incompletely recorded current derivative signals, whose peaks are well above the noise level, proved to be quite valuable for modelling purpose.

The paper proposes a double-term Pulse function that is investigated and compared with the double-term Heidler function for modelling the lightning return-stroke current. In the proposed paper, a complete large return-stroke current derivative signal recorded on June 10, 1996, is artificially cut. Then, each of the chosen double-term simulating functions is used to try to recover the original artificially cut signal for evaluating the proposed algorithm before applying it on signals that were incompletely recorded. The quality of fitting of the measured signal and the recovered signal are evaluated with R^2 fitting factor. Furthermore, the simulating functions are again used to recover incompletely-recorded return-stroke current derivative signals, which were measured on June 10, 1996.

The main objective of this study is to successfully recover the valuable incompletely-recorded signals, which are to be used for evaluation of tall-structure lightning models by comparing the simulated electric and magnetic fields with those measured [Rahimian and Hussein, 2015].

II. SIMULATING FUNCTIONS

The simulating functions, Heidler and the Pulse functions, each consists of a rise function $x(t)$ and a decay function $y(t)$. Rise and decay functions have a decoupling relationship with the condition that during the rise $y(t) \approx 1$ and during the decay $x(t) \approx 1$ [Heidler and Cvetic, 2002]. The general single-term current waveform of each simulation function is defined as:

$$i(t) = I_{max} \cdot x(t) \cdot y(t) \tag{1}$$

Mathematically, double-term Heidler current function and its derivative are defined as: [Milewski et al, 2008; Rahimian et al., 2015; Yazhou et al., 2002]

$$\begin{aligned} i(t) = I_1 \cdot \frac{\left(\frac{t}{\tau_{11}}\right)^{n_1}}{1+\left(\frac{t}{\tau_{11}}\right)^{n_1}} \cdot e^{-\frac{t}{\tau_{21}}} + \\ I_2 \cdot \frac{\left(\frac{t}{\tau_{12}}\right)^{n_2}}{1+\left(\frac{t}{\tau_{12}}\right)^{n_2}} \cdot e^{-\frac{t}{\tau_{22}}} \\ = i_1(t) + i_2(t) \end{aligned} \tag{2}$$

$$\begin{aligned} \frac{di(t)}{dt} = i_1(t) \cdot \left[\frac{n_1}{t} - \frac{1}{\tau_{21}} - \frac{n_1 t^{n_1-1}}{\left(\tau_{11}^{n_1} + t^{n_1}\right)}\right] + \\ i_2(t) \cdot \left[\frac{n_2}{t} - \frac{1}{\tau_{22}} - \frac{n_2 t^{n_2-1}}{\left(\tau_{12}^{n_2} + t^{n_2}\right)}\right] \end{aligned} \tag{3}$$

The proposed double-term Pulse function is defined in (4) and its derivative is given in (5).

$$\begin{aligned} i(t) = I_1 \cdot \left(1 - e^{-\frac{t}{\tau_{11}}}\right)^{n_1} \cdot e^{-\frac{t}{\tau_{21}}} + \\ I_2 \cdot \left(1 - e^{-\frac{t}{\tau_{12}}}\right)^{n_2} \cdot e^{-\frac{t}{\tau_{22}}} \\ = i_1(t) + i_2(t) \end{aligned} \tag{4}$$

$$\begin{aligned} \frac{di(t)}{dt} = i_1(t) \cdot \left[\frac{n_1}{\tau_{11}}\left(\frac{e^{-\frac{t}{\tau_{11}}}}{1 - e^{-\frac{t}{\tau_{11}}}}\right) - \frac{1}{\tau_{21}}\right] + \\ i_2(t) \cdot \left[\frac{n_2}{\tau_{12}}\left(\frac{e^{-\frac{t}{\tau_{12}}}}{1 - e^{-\frac{t}{\tau_{12}}}}\right) - \frac{1}{\tau_{22}}\right] \end{aligned} \tag{5}$$

To obtain the best fit for the measured current derivative waveform, the time derivative of Heidler and the Pulse functions are used here for the simulation. The current functions are then obtained by integrating the simulated current derivatives.

Some constraints are introduced to improve the fitting of each current derivative simulation as in [Milewski et al, 2008; Rahimian et al., 2015]. Constraints force the analytical parameters n_1, τ_{21}, τ_{11}, n_2, τ_{22}, and τ_{12} to reach their optimal values, which yields a better fit of the simulated current.

Forcing the maximum steepness constraint $\left.\frac{d^2 i}{dt^2}\right|_{t=t_{ms}} = 0$, where t_{ms} is the time at which the maximum steepness of the current or the time at which the maximum amplitude of the current derivative occurs. This constraint mentioned above provides the best fit [Elrodesly et al., 2012; Rahimian et al., 2015; Yazhou et al., 2002].

However, it was not possible to directly apply the maximum steepness constraint on the double-term Heidler function and obtain a closed expression for τ_{11} and τ_{12}. Therefore, the maximum steepness constraint is applied onto equation (2) to derive the following expressions.

$$\begin{aligned} f_h(t_{ms}) = i_1(t_{ms}) \cdot \left[\frac{n_1}{t_{ms}}\left(\frac{n_1 - 1}{t_{ms}} - \frac{2}{\tau_{21}}\right)\right. \\ + \frac{n_1 {t_{ms}}^{n_1-1}}{\tau_{11}^{n_1} + {t_{ms}}^{n_1}}\left(\frac{2n_1 {t_{ms}}^{n_1-1}}{\tau_{11}^{n_1} + {t_{ms}}^{n_1}} - \frac{3n_1 - 1}{t_{ms}} - \frac{2}{\tau_{21}}\right) \\ \left. + \frac{2}{{\tau_{21}}^2}\right] \end{aligned} \tag{6}$$

$$\begin{aligned} g_h(t_{ms}) = -\frac{\left(\frac{t}{\tau_{12}}\right)^{n_2}}{1+\left(\frac{t}{\tau_{12}}\right)^{n_2}} \cdot e^{-\frac{t}{\tau_{22}}} \\ \cdot \left[\frac{n_2}{t_{ms}}\left(\frac{n_2 - 1}{t_{ms}} - \frac{2}{\tau_{22}}\right) + \frac{n_2 {t_{ms}}^{n_2-1}}{\tau_{11}^{n_2} + {t_{ms}}^{n_2}}\right. \\ \left.\left(\frac{2n_2 {t_{ms}}^{n_2-1}}{\tau_{11}^{n_2} + {t_{ms}}^{n_2}} - \frac{3n_2 - 1}{t_{ms}} - \frac{2}{\tau_{22}}\right) + \frac{2}{{\tau_{22}}^2}\right] \end{aligned} \tag{7}$$

$$I_2 = \frac{f_h(t_{ms})}{g_h(t_{ms})} \tag{8}$$

Then, the expression for I_2 is substituted into (3) to acquire the final expression (9), which is used in the fitting process.

$$\begin{aligned} \frac{di(t)}{dt} = i_1(t) \cdot \left[\frac{n_1}{t} - \frac{1}{\tau_{21}} - \frac{n_1 t^{n_1-1}}{\left(\tau_{11}^{n_1} + t^{n_1}\right)}\right] + \\ \frac{f_h(t_{ms})}{g_h(t_{ms})} \cdot \left[\frac{n_2}{t} - \frac{1}{\tau_{22}} - \frac{n_2 t^{n_2-1}}{\left(\tau_{12}^{n_2} + t^{n_2}\right)}\right] \end{aligned} \tag{9}$$

For the double-term Pulse function, the same procedure is applied onto equation (4) to derive the following expressions.

$$\begin{aligned} f_p(t_{ms}) = i_1(t) \cdot \left[\left(\frac{n_1}{\tau_{11}}\left(\frac{e^{-\frac{t}{\tau_{11}}}}{1 - e^{-\frac{t}{\tau_{11}}}}\right)\right)^2 - \right. \\ \left. \frac{2n_1}{\tau_{11}\tau_{21}}\left(\frac{e^{-\frac{t}{\tau_{11}}}}{1 - e^{-\frac{t}{\tau_{11}}}}\right) + \frac{1}{{\tau_{21}}^2} - \frac{n_1}{{\tau_{11}}^2}\left(\frac{e^{-\frac{t}{\tau_{11}}}}{\left(1 - e^{-\frac{t}{\tau_{11}}}\right)^2}\right)\right] \end{aligned} \tag{10}$$

$$g_p(t_{ms}) = \left(1 - e^{-\frac{t}{\tau_{12}}}\right)^{n_2} \cdot e^{-\frac{t}{\tau_{22}}} \cdot \left[\left(\frac{n_1}{\tau_{11}}\left(\frac{e^{-\frac{t}{\tau_{11}}}}{1 - e^{-\frac{t}{\tau_{11}}}}\right)\right)^2 - \frac{2n_1}{\tau_{11}\tau_{21}}\left(\frac{e^{-\frac{t}{\tau_{11}}}}{1 - e^{-\frac{t}{\tau_{11}}}}\right) + \frac{1}{{\tau_{21}}^2} - \frac{n_1}{{\tau_{11}}^2}\left(\frac{e^{-\frac{t}{\tau_{11}}}}{\left(1 - e^{-\frac{t}{\tau_{11}}}\right)^2}\right)\right] \quad (11)$$

$$I_2 = \frac{f_p(t_{ms})}{g_p(t_{ms})} \quad (12)$$

Equation (12) is substituted into (5) to derive the final expression (13), which is to be used in the fitting process.

$$\frac{di(t)}{dt} = i_1(t) \cdot \left[\frac{n_1}{\tau_{11}}\left(\frac{e^{-\frac{t}{\tau_{11}}}}{1 - e^{-\frac{t}{\tau_{11}}}}\right) - \frac{1}{\tau_{21}}\right] + \frac{f_p(t_{ms})}{g_p(t_{ms})} \cdot \left[\frac{n_2}{\tau_{12}}\left(\frac{e^{-\frac{t}{\tau_{12}}}}{1 - e^{-\frac{t}{\tau_{12}}}}\right) - \frac{1}{\tau_{22}}\right] \quad (13)$$

III. METHODOLOGY

One of the multi-stroke CN tower flashes, recorded on June 10, 1996, is utilized in this paper for modelling. The 6th and 7th return-stroke current derivative signals are used for modelling due to their high current derivative peaks. 7th return-stroke current derivative signal is incompletely-recorded, which is to be used for the recovery process.

A. Matching Waveforms

For the fitting process, the starting point of the current derivative waveform is chosen from the measured lightning return-stroke current waveform [Milewski, 2008]. Fig. 1 illustrates the 6th return-stroke current derivative signal. The initial point is assumed to be at $t = -0.21\ \mu s$ for modelling purpose.

The matching waveforms are then divided into three time-windows. The decoupling relationship of Heidler and Pulse functions allow the signal to be easily divided into sections [Elrodesly et al., 2012]. The three time windows are:

1. The initial impulse before arrival of reflections (Fig.2)
2. The reflections and early decay part of the waveform
3. The decay portion is based on the current waveform (Fig. 3)

Figure 2 illustrates the first time window of the 6th current derivative matching signal. The duration of the first time window is $t = 0 - 0.6\ \mu s$ because the reflection from the space deck is visible after $t = 0.6\ \mu s$ [Rahimian et al., 2015].

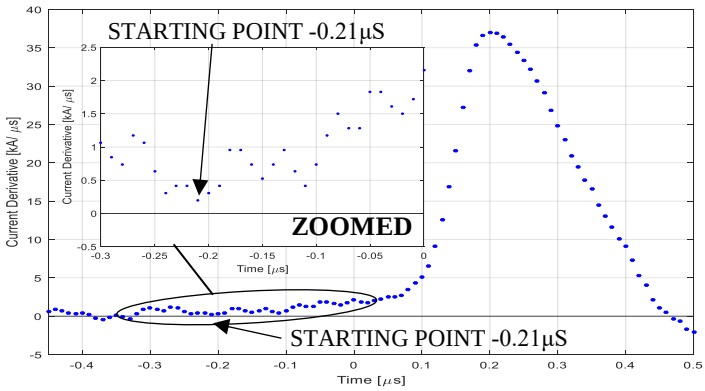

Fig. 1. 6th current derivative waveform. Zoomed-in view illustrates the starting point at which di(t)/dt ≈ 0

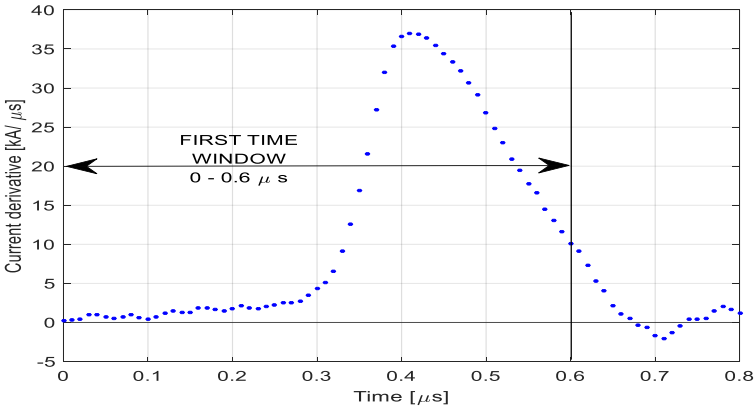

Fig. 2. The first time window of the 6th current derivative matching signal

Figure 3 illustrates the third time windows of the 6th return-stroke current waveform obtained by numerically integrating its current derivative matching waveform. This time window is used to estimate τ_{21} and τ_{22}, as explained in section B.

B. Estimating τ_{21} and τ_{22}

First step in approximating the analytical parameters is to estimate the decay time constants τ_{21} and τ_{22}. During the decay portion, both simulating functions are simplified to:

$$i(t) = I_1 \cdot e^{-\frac{t}{\tau_{21}}} + I_2 \cdot e^{-\frac{t}{\tau_{22}}} \quad (14)$$

τ_{21} and τ_{22} can be estimated by fitting the decay function described by (14) into a chosen third time window, using MATLAB. For the 6th return-stroke current waveform, using the third-time window described in Fig. 3, it was found that $\tau_{21} = 0.09754\ \mu s$, $\tau_{22} = 110\ \mu s$, $I_1 = 0.2785\ kA$, and $I_2 = 9.834\ kA$ with R^2 fitting of 0.9325, indicating a good fit. The fitting process is illustrated in Fig. 3.

IV. RESULTS

The derivative of Heidler and the Pulse functions described by (9) and (13), respectively, are used in fitting the 6th current derivative matching waveform. The fitting is conducted using MATLAB Fitting Toolbox to estimate the unknowns, I_1, n_1, τ_{21}, τ_{11}, n_2, τ_{22} and τ_{12}.

The fittings of Heidler and Pulse functions obtained for the 6th current derivative matching waveform and its current waveform are illustrated in Figs. 4 and 5, respectively. The analytical parameters obtained for the waveform is summarized in Table I along with the R^2 fitting factors.

In Fig. 4, t_{ms} of the current derivative of Heidler function matches t_{ms} of the 6th current derivative matching waveform, which was attained using the maximum steepness constraint, whereas the maximum derivative of the Pulse function is shifted to the right by 0.005μs. The location of the current derivative peak based on Heidler function is found to be closer to the measured peak in comparison with that based on the Pulse function.

Table I indicates that the simulation based on the derivative of the Pulse and Heidler functions produced excellent fittings of $R^2 = 0.9975$ and $R^2 = 0.998$, respectively. The simulation based on the Heidler function produced a slightly better fit than that based on the Pulse function. Furthermore, the location of the maximum current derivative peak based on Heidler function simulation is much closer than that using the Pulse function (Fig. 4). The maximum amplitude of the 6th current derivative matching waveform is 36.97 kA/μs, whereas that estimated from the derivative of Heidler function is 38kA/μs. However, the derivative of the Pulse function is estimated to be 37.45kA/μs. Thus, the maximum current derivative peak based on the Pulse function simulation is closer to the measurement than that using Heidler function (Fig. 4).

Figure 5 indicates that the peak of the 6th return-stroke current waveform was not reached by Heidler and the Pulse functions. But the Heidler current function has a minor overshoot compared with that of the Pulse function. Observing Fig. 5, shows that the Pulse function reaches the current peak slower in comparison with the Heidler function. Both Heidler and the Pulse functions reasonably simulated the measurement.

One of the biggest challenges faced by many researchers is the incompletely-recorded return-stroke current derivative signals, which exceeded the maximum signal set levels [Rahimian, and Hussein, 2015]. These incompletely-recorded return-stroke current derivative signals, such as the 7th return-stroke current derivative signal, which will be further investigated in this paper, whose peaks are well above the noise level, proved to be quite valuable for modelling purpose.

Prior to starting the recovery of the incompletely-recorded 7th return-stroke current derivative signal, a completely recorded signal with negligible amount of noise, the 6th return-stroke current derivative signal is artificially cut and the recovery process is applied on it (Fig. 6).

The measured data of the 6th return-stroke current derivative within the interval $0.35\mu s < t < 0.55\mu s$ is removed to obtain a waveform that is artificially cut at the 50% level from the peak, as illustrated in Fig. 6. The same methodology described using the 6th return-stroke current derivative matching waveform is followed to fit the simulating functions for the artificially-cut 6th current derivative waveform. The fitting results obtained for the artificially-cut 6th current derivative waveform and its current waveform are illustrated in Figs. 6 and 7, respectively. The analytical parameters obtained for this waveform is summarized in Table II along with the R^2 fitting factors.

The recovery of the artificially-cut 6th current derivative waveform is obtained by using the current derivative of the Pulse function. It is found to be more successful in the recovery of the artificially-cut 6th current derivative waveform compared with the current derivative of Heidler function.

In Fig. 6, t_{ms} of the current derivative of the Pulse waveform, which was attained using the maximum steepness constraint, is shifted to the right by 0.02μs. Table I indicates that the simulation based on the derivative of the Pulse function produced an excellent fitting of $R^2 = 0.9955$. Furthermore, the time location of the current derivative peak, based on the Pulse function (Fig.6), is close to the location of the measured current derivative peak. Furthermore, the maximum amplitude of the 6th current derivative measured waveform is 36.97 kA/μs and the recovery using the derivative of the Pulse function estimated peak is 36.52kA/μs. Thus, the maximum current derivative peak based on the Pulse function simulation is proved to be close to the measured data.

Figure 7 indicates that the peak of the 6th return-stroke current waveform was not reached by the Pulse function. It has a minor overshoot. However, the Pulse function reasonably recovered the measurement data.

The same methodology described using the artificially-cut 6th return-stroke current derivative matching waveform is followed to fit the simulating functions for 7th return-stroke current derivative waveform, the incompletely-recorded signal. The recovery of incompletely-recorded signal is obtained using the current derivative of Heidler function. It is found to be more successful in the recovery process compared with the current derivative of the Pulse function. The fitting results obtained for the 7th return-stroke current derivative waveform is illustrated in Fig. 8. The analytical parameters obtained for this waveform is summarized in Table II along with the R^2 fitting factors.

In Fig. 8, t_{ms} of the current derivative of Heidler waveform match t_{ms} of the 7th current derivative matching waveform, which was attained using the maximum steepness constraint. Table II indicates that the simulation based on the derivative of Heidler function produced an excellent fitting of $R^2 = 0.9843$. The maximum amplitude of the 7th current derivative waveform estimated by Heidler function is 140.1kA/μs. Thus, the Heidler function simulation is very close to the measured data and reasonably recovered missing data.

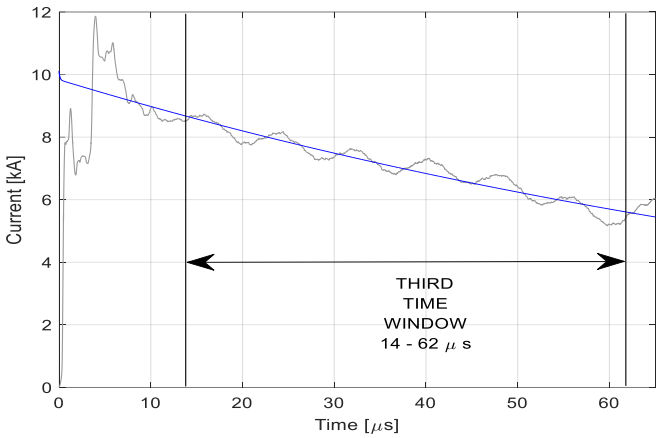

Fig. 3. Third time window of the 6th return-stroke current waveform and the fitting of the decay function described by (12), which is used to estimate τ_{21} and τ_{22}.

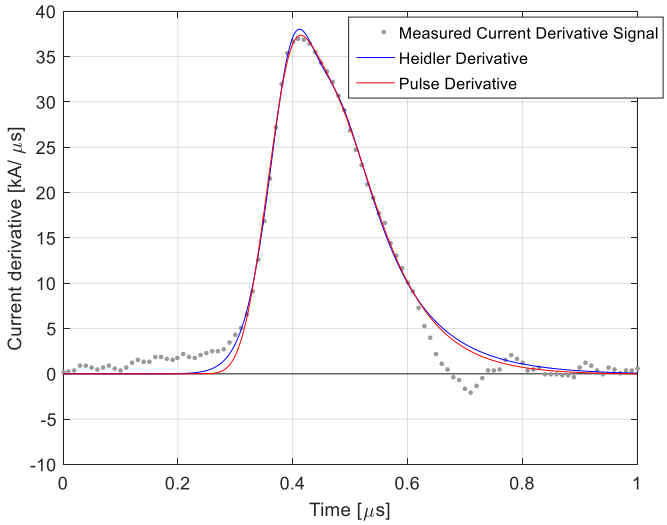

Fig. 4. The fitting of Heidler and Pulse derivative functions of the 6th current derivative matching waveform.

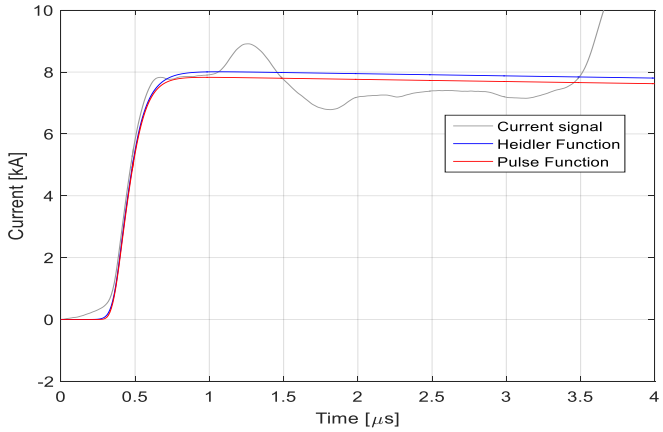

Fig. 5. The fitting of Heidler and Pulse functions of the 6th current waveform (obtained by numerically integrating the 6th current derivative matching waveform).

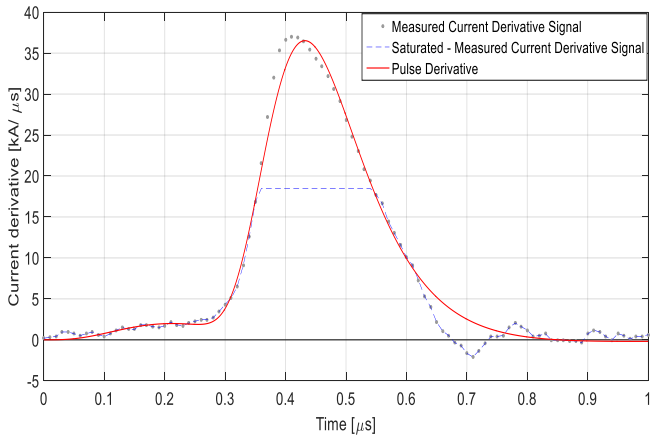

Fig. 6. The fitting of the Pulse derivative function of the artificially cut 6th current derivative waveform.

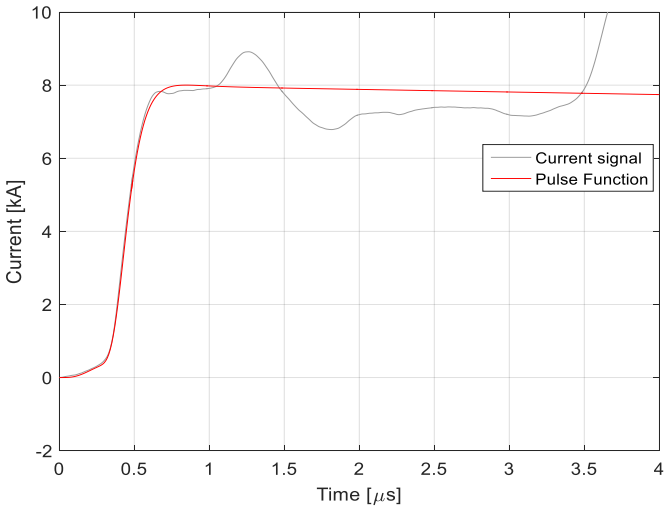

Fig. 7. The fitting of the Pulse function of the artificially cut 6th current waveform (obtained by numerically integrating).

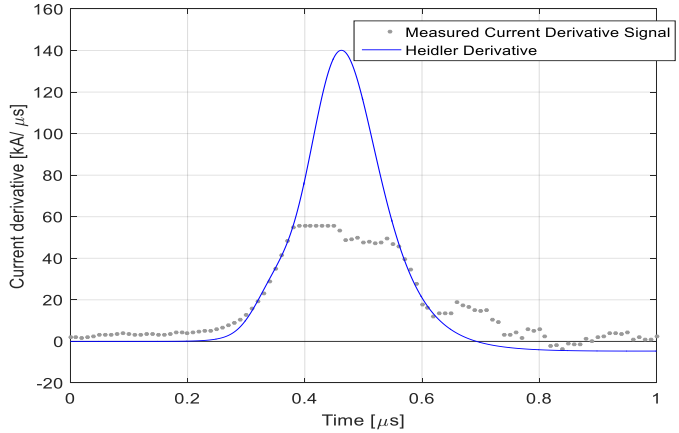

Fig. 8. The fitting of Heidler derivative function of the 7th current derivative waveform (incompletely recorded waveform).

V. CONCLUSION

Following numerous investigations, researchers found out that Heidler and the Pulse functions overcome a lot of limitations experienced by the double-exponential and Jones modified double-exponential functions.

The paper presented a comparison between Heidler and the Pulse functions for modelling the lightning return-stroke current, using the 6th return-stroke current derivative waveform measured on June 10th 1996 at the CN tower. A complete large return-stroke current derivative signal is artificially-cut at the 50% level from the peak. Then, each of the chosen double-term simulating functions are used to try to recover the original artificially-cut signal for evaluating the proposed algorithm before applying it on 7th return-stroke current derivative waveform, was not a completely recorded signal.

With the 6th current derivative matching waveform, the derivative of the Pulse and Heidler functions produced exceptional fittings of $R^2 = 0.9975$ and $R^2 = 0.998$, respectively. With the artificially-cut 6th current derivative waveform, the derivative of the Pulse function found to be successful in the recovery process and produced $R^2 = 0.9955$. Using the 7th return-stroke current derivative waveform, the derivative of Heidler function is found to be more successful in the recovery process and produced $R^2 = 0.9843$. Both Heidler and Pulse simulation functions can successfully simulate tall-structure lightning return-stroke currents and recover valuable missing data.

ACKNOWLEDGMENT

This work was funded in part by the Natural Sciences and Engineering Research Council of Canada, NSERC Discovery Grant (2012-2017), which is gratefully acknowledged. The authors also acknowledge Ryerson University internal funding and facilities.

REFERENCES

Elrodesly, K., and A.M.Hussein (2012), Cn Tower Lightning Return-Stroke Current Simulation, Journal of Lightning Research, 4, pp. 60-70.

Heidler, F., and J. Cvetic (2002), A Class of Analytical Functions to Study the Lightning Effects Associated With the Current Front, European Transactions on Electrical Power, 12(2), pp. 141-150.

Hussein, A.M. (2009), Current waveform characteristics of negative and positive lightning to the CN Tower, Proceedings X International Symposium on Lightning Protection, SPIDA, Curitiba, Brazil, pp. 451-456.

Hussein, A.M., S. Kazazi, M. Anwar, M. Yusouf and P. Liatos (2014), CN Tower Lightning Characteristics Based on Current-Recorded Flashes, Proceedings International Conference on Lightning Protection, ICLP, Shanghai, China, pp. 2028-2034.

Hussein, A.M., W. Janischewskyj, J.S. Chang, V. Shostak, W.A. Chisholm, P. Dzurevych, and Z.I. Kawasaki (1995), Simultaneous measurement of lightning parameters for strokes to the Toronto Canadian National Tower, Journal of Geophysical Research, 100(5), pp. 8853-8861.

Janischewskyj, W., A.M. Hussein, V. Shostak, I. Rusan, J.X. Li, and J.S. Chang (1997), Statistics of Lightning Strikes to the Toronto Canadian National Tower (1978-1995), IEEE Transaction on Power Delivery, 12(3), pp. 1210-1221.

Jones, R.D. (1977), On the Use of Tailored Return-Stroke Current Representations to Simplify the Analysis of Lightning Effects on Systems, IEEE Transactions on Electromagnetic Compatibility, 19(2), pp. 95-96.

Liatos, P., and A.M. Hussein (2005), Characterization of Noise in the Lightning Current Derivative Signals Measured at the CN Tower, IEEE Transaction on Electromagnetic Compatibility, 47(4), pp. 986-997.

Milewski, M., and A. M. Hussein (2008), Lightning return-stroke transmission line model based on CN tower lightning data and derivative of heidler function,Canadian Conference on Electrical and Computer Engineering, CCECE, Niagara Falls, Canada, pp. 001861–001866

Nedjah, O., A.M. Hussein, S. Krishnan and R. Sotudeh (2010), Comparative study of adaptive de-noising techniques for lightning current derivative signals, European Association for Signal Processing (EURASIP) Journal, 20(2), pp. 607-618.

Rahimian, M.S., and A.M. Hussein (2015), ATP Modeling of Tall-Structure Lightning Current: Estimation of Return-Stroke Velocity Variation and Upward-Connecting Leader Length, IEEE Transaction on Electromagnetic Compatibility, 57(6), pp. 1576-1592.

Rakov, V.A., and M.A. Uman (2003), Lightning: Physics and Effects, Cambridge Univ. Press, New York.

Uman, M.A. (1971), All about lightning, Dover Publications, New York.

Yazhou, C., L. Shanghe, W. Xiaorong, and Z. Feizhou (2002), A New Kind of Lightning Channel-base Current Function, Proceedings 3rd International symposium on Electromagnetic Compatibility, Beijing, China, pp. 304-307.

TABLE I. HEIDLER AND PULSE FUNCTIONS FITTING RESULTS AND R^2 FITTING FACTOR

	6th Current Derivative Matching Waveform									
	I_1[kA]	η_1	η_2	τ_{11}[µs]	τ_{12}[µs]	τ_{21}[µs]	τ_{22}[µs]	n_1	n_2	R^2
Heidler	9.989	1.234	0.01011	0.4164	0.4484	110	0.09754	12.25	13.98	0.998
Pulse	8.136	1.029	1.43	0.0723	0.04226	110	0.09754	361.2	6.191e+04	0.9975

TABLE II. FITTING RESULTS AND R^2 FITTING FACTOR

	I_1[kA]	η_1	η_2	τ_{11} [µs]	τ_{12} [µs]	τ_{21} [µs]	τ_{22} [µs]	n_1	n_2	R^2
Artificially Cut 6th Current Derivative Waveform (Pulse)	7.051e+4	1.526	0.1128	1.859	0.07991	110	0.09754	4.577	227.6	0.9955
7th Current Derivative Waveform (Heidler)	8.136	0.0553	22.59	0.4695	14.61	4.623	0.003905	11	95.33	0.9843